UC Santa Barbara
UC Santa Barbara Previously Published Works

Title

Distinguishing barriers and asperities in near-source ground motion

Permalink

https://escholarship.org/uc/item/2bf3f9bn

Journal

Journal of Geophysical Research-Solid Earth, 110(B11)

ISSN

0148-0227

Authors

Page, Morgan T
Dunham, E M
Carlson, J M

Publication Date

2005-11-01

DOI

10.1029/2005JB003736

Peer reviewed

Distinguishing Barriers and Asperities in Near-Source Ground Motion

Morgan T. Page

Department of Physics, University of California at Santa Barbara, Santa Barbara, California, USA

Eric M. Dunham

Department of Physics, University of California at Santa Barbara, Santa Barbara, California, USA

Department of Earth and Planetary Sciences, Harvard University, Cambridge, Massachusetts, USA

J. M. Carlson

Department of Physics, University of California at Santa Barbara, Santa Barbara, California, USA

Abstract. We investigate the ground motion produced by rupture propagation through circular barriers and asperities in an otherwise homogeneous earthquake rupture. Using a three-dimensional finite-difference method, we analyze the effect of asperity radius, strength, and depth in a dynamic model with fixed rupture velocity. We gradually add complexity to the model, eventually approaching the behavior of a spontaneous dynamic rupture, to determine the origin of each feature in the ground motion. A barrier initially resists rupture, which induces rupture-front curvature. These effects focus energy on and off the fault, leading to a concentrated pulse from the barrier region and higher velocities at the surface. Finally, we investigate the scaling laws in a spontaneous dynamic model. We find that dynamic stress drop determines fault-parallel static offset, while the time it takes the barrier to break is a measure of fracture energy. Thus, given sufficiently strong heterogeneity, the prestress and yield stress (relative to sliding friction) of the barrier can both be determined from ground-motion measurements. In addition, we find that models with constraints on rupture velocity have less ground motion than constraint-free, spontaneous dynamic models with equivalent stress drops. This suggests that kinematic models with such constraints overestimate the actual stress heterogeneity of earthquakes.

1. Introduction

Heterogeneity plays an important role in earthquake rupture propagation. Stored stress, strength, and frictional properties on the fault plane conspire to yield a complex rupture process. Numerous kinematic inversions of waveform data indicate that earthquake ruptures follow complex paths and have heterogeneous slip distributions [*Hartzell and Heaton*, 1983; *Archuleta*, 1984; *Beroza and Spudich*, 1988; *Wald and Heaton*, 1994; *Cotton and Campillo*, 1995]. The purpose of this paper is to examine aspects of ground motion in the context of simple but heterogeneous ruptures.

Kinematic inversions employ the dislocation model, which describes the earthquake as propagating slip along a fault plane. The displacement u recorded by a seismograph on the surface can then be written as

$$u_i(\vec{x}, t) = \int_0^t \int_\Sigma \Delta u_j(\vec{\xi}, \tau)\, G_{ij}(\vec{x} - \vec{\xi}, t - \tau)\, d\vec{\xi}\, d\tau, \quad (1)$$

where Δu is the slip on the fault surface Σ, and G is the Green's function for a point dislocation and a given fault and crustal structure. Note that matching $u(\vec{x}, t)$ on the surface does not guarantee that the slip propagation is physical. For example, simple dislocation models can produce infinite accelerations and infinite stress drops [*Madariaga*, 1978]. In addition, this is an underdetermined problem, as Δu on the fault is not unique for a given u on the surface. The displacement u is only known at a limited number of stations, and their proximity to the fault limits the frequency resolution of Δu. In the far-field, the inverse problem is unstable, as slip distributions with arbitrarily different L_2 norms can produce identical radiation [*Kostrov and Das*, 1988]. Constraints must be introduced into the inverse problem to overcome this instability. Consequently, most kinematic inversions that use the dislocation model assume constant rupture velocity or constrain the rupture velocity to be slowly varying [*Olson and Apsel*, 1982; *Hartzell and Heaton*, 1983].

While the kinematic approach specifies slip everywhere on the fault, dynamic modeling of an earthquake is formulated as a mixed boundary-value problem, with slip and stress specified on different parts of the fault. In the case of a highly nonuniform rupture velocity, this mixing of boundary conditions prevents the linearization of the dynamic inverse problem. While nonlinear dynamic inversions have been attempted [*Peyrat et al.*, 2004], they require extensive computational resources and currently have poor resolution. Thus, kinematic modeling remains the most widely used tool with which to match observed waveforms.

As dynamic inversions are not yet practical, it is extremely important to understand the dynamic effects associated with heterogeneities. Do kinematic inversions capture heterogeneity in a way that is compatible with what we know about dynamic, physically realistic rupture propagation? What type of radiation do we expect to see from inhomogeneities in dynamic rupture? Since kinematic inversions are poorly constrained, forward modeling is needed to ensure that dynamic effects are captured in a physically consistent way.

In this paper, we analyze the radiation produced by circular barriers and asperities in an otherwise homogeneous rupture. The terms "barrier" and "asperity" are widely used in a variety of contexts, but in this paper we define them as in *Madariaga* [1983], in reference to the dynamic parameters on the fault. We define a barrier as a region that has a higher frictional strength (yield stress) than the surrounding fault. Real-life barriers can be regions with different material properties or changes in the fault geometry that hinder rupture propagation. An asperity is a region with a higher prestress than the surrounding fault, while an anti-asperity has a lower prestress. Note that the term "asperity" is used in the kinematic-modeling community to denote a region with high slip, but here we use it to refer to stress level. Asperities may be regions that remained unbroken during a previous earthquake and thus are closer to failure. Asperities and barriers produce different ground motion, as barriers delay rupture but asperities do not. A region can, of course, have both an increased prestress and yield stress, and be both an asperity and a barrier in this sense.

Das and Kostrov [1983] first studied the breaking of a single circular asperity and found that rupture initially circled the edges of the asperity before collapsing inward. Later, *Fukuyama and Madariaga* [2000] also analyzed the single asperity with higher resolution. In recent work, *Dunham et al.* [2003] studied the spontaneous, dynamic propagation of rupture around a barrier and an anti-asperity. While both of these obstacles delay rupture, they interact quite differently with the rupture front. In the case of the barrier, this region initially resists rupture, slowing down the rupture front. The rupture front surrounds the region, focusing waves into the barrier. This phenomena, in which a curved rupture front focuses waves, is termed rupture-front focusing [*Fukuyama and Madariaga*, 2000]. This focusing can eventually cause the barrier region to rupture. In some cases the barrier failure can initiate supershear rupture, in which the rupture velocity exceeds the shear wave speed [*Dunham et al.*, 2003]. This is an important test case because it isolates the interactions between heterogeneities and the rupture front that lead to phenomena that would not be captured without a complete, dynamic description. While the work of *Dunham et al.* [2003] focused on the propagation of the rupture on the fault, in this paper we will primarily be investigating the ground motion produced by these heterogeneities.

In order to better understand the radiation associated with the dynamic breaking of a barrier or asperity, we develop a series of models with increasing levels of complexity. These models have various assumptions, designed to capture and separate the key phenomena observed in fully dynamic simulations. In this way, the effects of rupture velocity, rupture front curvature, and time to break the barrier – all of which arise in the fully spontaneous, dynamic, inhomogeneous rupture – can be separated and studied. The models are summarized in Table 1 and are of two varieties: reduced and spontaneous, as described below. The medium surrounding the fault is isotropic and linear elastic, with identical material properties on each side. The shear modulus is $\mu = 30$ GPa, the S-wave speed is $c_s = 3.46$ km/sec, and Poisson's ratio is 1/4. We constrain slip to be horizontal, which renders the frictional dynamics insensitive to the absolute level of stress. This allows us to measure all stresses with respect to sliding friction. This convention is used hereafter; for example, the terms prestress and yield stress refer to the difference between these values and sliding friction. The fault is 20 km long and extends from the free surface to 10 km depth. The heterogeneity is located 10 km along strike.

We initially analyze several reduced models in terms of their effects on ground motion. These models are reduced in the sense that the rupture velocity is constrained, so that they are not spontaneous. They are, however, dynamic, as we specify shear traction on the slipping part of the fault. The first model, Model A, constrains the rupture velocity to be constant everywhere, even in the zone of heterogeneity. The only heterogeneity in this model is the extra stress drop in the circular zone. Also, the rupture front is straight, as shown in Figure 1. In the second reduced model, Model B, the breaking of the heterogeneity is delayed, as is seen in spontaneous, dynamic models [*Das and Aki*, 1977]. The circular zone, which is now more like a barrier, ruptures in the same manner as in Model A (with a straight rupture front within the heterogeneity), but at a later time. In Model C, we better approximate the way in which the barrier fails by adding curvature to the rupture front, which enhances rupture-front focusing. Finally, we analyze the spontaneous, fully dynamic model, complete with the effects of variable rupture velocity and rupture-front focusing. In this model, Model D, we find that with sufficient resolution of only two
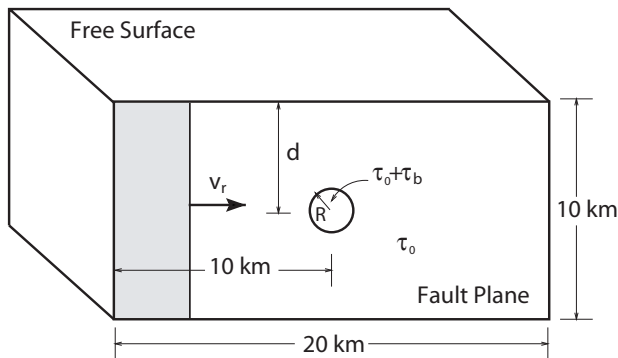

Figure 1. Reduced model parameters. Rupture is initiated on a vertical patch at the left side of the right-lateral strike-slip fault plane. The rupture front travels to the right with a fixed rupture velocity of v_r, eventually reaching a circular heterogeneity of radius R at a depth d. Most of the fault has a prestress of τ_0, while the circular region in the center of the fault has a prestress of $\tau_0 + \tau_b$.

Table 1. Models at various stages of complexity.

| Model	Description	Effects
A	Dynamic model with fixed rupture velocity throughout, even in barrier.	Additional displacement proportional to $R^2 \tau_b$.
B	Dynamic model with fixed rupture velocity. Barrier ruptures at a later time, but in identical manner to Model A.	Stopping phases from barrier lead to initial arrest of ground motion, followed by larger peak velocities on surface when barrier finally breaks.
C	Dynamic model with fixed rupture velocity and barrier time delay. Barrier ruptures with curved rupture front.	Curved rupture front focuses energy, leads to more well-defined barrier pulse.
D	Spontaneous dynamic model (rupture velocity is no longer fixed). Can now vary prestress and yield stress independently.	Similar to Model C, but with increased focusing effect. Also, unconstrained rupture velocity leads to more radiation than with non-spontaneous models.
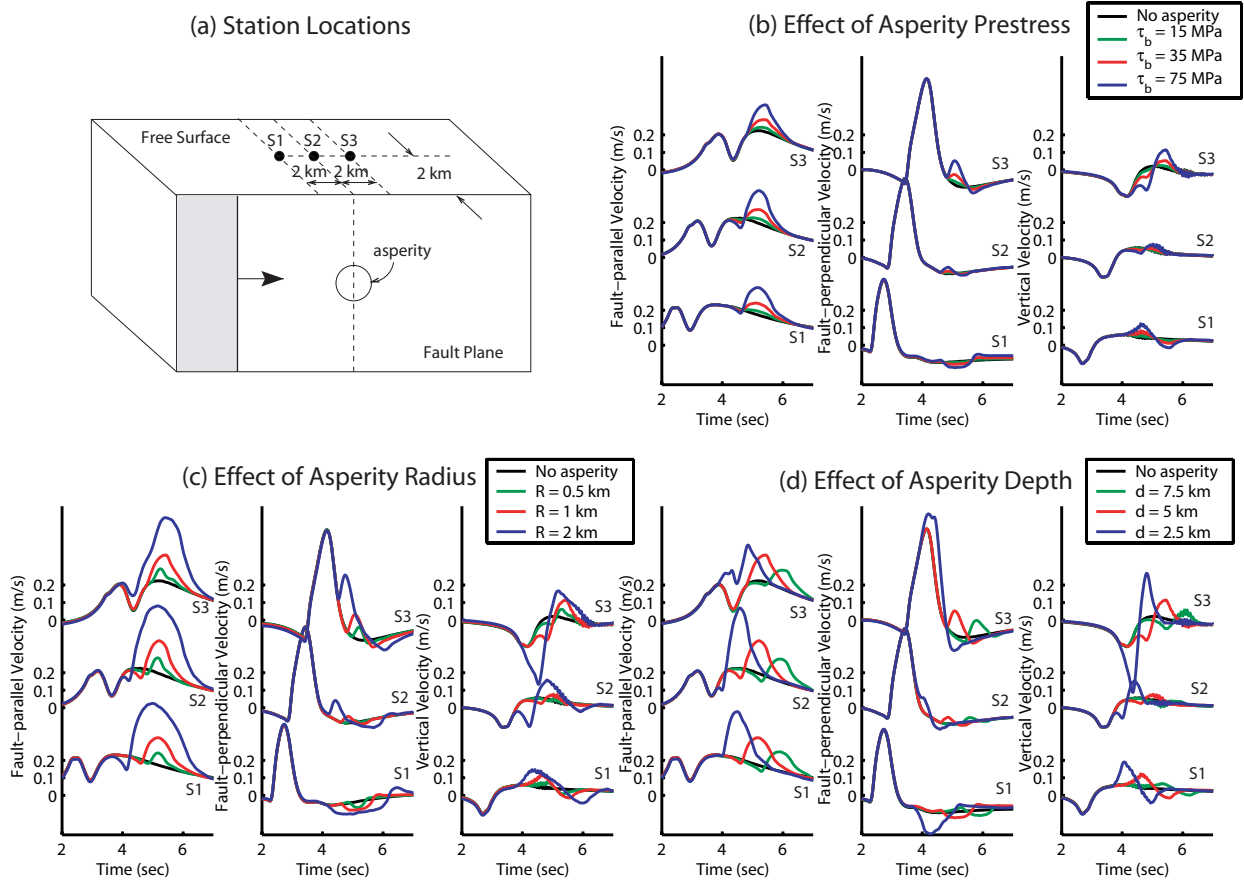
Figure 2. Effect of asperity prestress, radius, and depth for a model with fixed rupture velocity and no barrier time delay (Model A) at three stations. The asperity pulses are most cleanly seen on the fault-parallel and vertical components, as the fault-normal components of the homogeneous rupture are larger, tending to drown out the barrier signal. Model A is linear, so the additional displacement due to the asperity scales with τ_b and R^2. In addition, the velocity pulse width increases with R and d. Note that the polarity of the fault-perpendicular and vertical asperity pulses give the location of the asperity: for example, in the fault-perpendicular record the first motion is towards the fault in the backwards direction from the asperity and away from the fault in the forward direction of the asperity on the right-moving block.

parameters in the ground motion, the prestress and fracture energy of the heterogeneity can be determined. This is in contrast to the general case in real, fully heterogeneous ruptures, where due to nonuniqueness we can invert for prestress or fracture energy, but not both independently everywhere [*Peyrat et al.*, 2001; *Guatteri and Spudich*, 2000]. In addition, we find that Model D – free of constraints on the rupture velocity – produces larger pulses in the ground motion than the reduced models with an equivalent stress drop. This is explained further in Section 3.

2. Reduced Models

In Models A, B, and C, we follow the method of *Andrews* [1985] to constrain rupture velocity to be constant in the context of a dynamic source representation. We want to keep the fault locked ahead of the rupture front, specify dynamic stress drop behind the rupture front, and solve for slip. We numerically regularize this singular problem by specifying frictional strength for each point on the fault as a function of time and position. This is similar to the cohesive-zone model of *Palmer and Rice* [1973]. Frictional strength for a given point at horizontal distance x from the

nucleation zone and at time t is given by

$$\tau_y = \begin{cases} 0 & \text{if } |x| < tv_r, \text{ and} \\ \frac{\tau_0}{2\Delta x}(|x| - v_r t) & \text{if } |x| > tv_r, \end{cases} \quad (2)$$

where v_r is the rupture velocity, τ_0 is prestress, and $\Delta x = 100$ m is the grid spacing. The slip-time function is not constrained as in a kinematic model. Rather, this is a dynamic (though not spontaneous) model that constrains rupture velocity, specifies stress, and solves for slip. Note that in this formulation stress drops linearly with distance on the fault, not with displacement, as with a slip-weakening friction law.

We parametrize the problem as follows: We specify the background prestress $\tau_0 = 5$ MPa, barrier prestress $\tau_0 + \tau_b$, barrier radius R, and barrier depth d, as shown in Figure 1. We specify a rupture velocity of 0.8 times the Rayleigh wave speed, which is a typical rupture velocity seen in real earthquakes [*Geller*, 1976; *Somerville et al.*, 1999]. Rupture begins along a vertical patch at one side of the fault.

In the first reduced model, Model A, the rupture velocity is constant everywhere on the fault, including in the circular heterogeneity itself. The heterogeneity in Model A is similar to an asperity rather than a barrier, as it does not delay the rupture front. Synthetic seismograms for this model with various values of τ_b, R, and d are shown in Figure 2, along

with the seismograms for a homogeneous rupture (no asperity) for comparison. The default parameters for the asperity in Figure 2 are $\tau_b = 35$ MPa, $R = 1$ km, and $d = 5$ km, unless otherwise stated. After subtracting off the displacements from the homogeneous rupture, this model cleanly shows that all components of additional displacement are proportional to R^2 and τ_b, for all points on the surface, at all times. This is to be expected as Model A is linear in the displacement and stress fields. Since the rupture front is always in the same location as in a homogeneous rupture, we can superpose the displacement from the homogeneous rupture with the displacement from the additional stress drop in the asperity region to give us the ground motion for Model A. Thus $R^2\tau_b$ is the effective force of the asperity [*Kostrov and Das*, 1988]. The scaling relationship for depth is more complicated, but this parameter has the most influence on surface displacement directly above the asperity. In addition, this model shows that velocity pulse width is independent of τ_b. The width of the asperity velocity pulse does increase with R and d, most notably in the forward direction from the asperity.

The pulses from the asperity are most easily seen in the fault-parallel and vertical records, as the background radiation in the fault-perpendicular records obscures them. One can use the height of the pulse to constrain R and τ_b, and the width of the pulse to constrain d and R. In addition, the polarity of the fault-perpendicular asperity pulses gives the location of the heterogeneity, as the first motion is towards the fault in the backward direction from the asperity and away from the fault in the forward direction from the asperity on the right-moving block. Directly above the asperity, asymmetry of the fault-normal component in the fault-parallel direction causes this pulse to vanish. The vertical records also show a reversal of polarity. If the asperity is large enough to resolve in the perpendicular or vertical component and there are enough near-field stations, the horizontal location of the heterogeneity can be determined by looking at the polarity of the asperity pulse relative to station location, as well as the pulse's absence in stations above the asperity.

In our second reduced model, Model B, we include an effect seen in spontaneous, dynamic models: a barrier time delay. Before we discuss the results of Model B, we first motivate this model by discussing results from spontaneous dynamic models, in which we find that the barrier breaks only after a time delay that increases with the additional resistance of the barrier. To quantify this effect, we first study the problem in the simple whole-space geometry (to remove the effects of the finite fault width and free surface) using a slip-weakening fracture criterion [*Ida*, 1972; *Palmer and Rice*, 1973; *Andrews*, 1976]. The initial rupture is bilaterally expanding with a straight front under mode II conditions (numerically accomplished by placing periodic boundary conditions in the vertical direction, as in *Dunham et al.* [2003]), and is perturbed into mixed-mode conditions as it encounters the barrier. We define the break time t_b as the difference between the time at which the rupture arrives at the closest point on the edge of the barrier and the time at which the last point within the barrier breaks. To quantify the resistance of the barrier, we take the fracture energy of the barrier $G_b = \tau_y^b d_c$ and scale it by the energy release rate of a static mode II crack having half-length L (measured to the center of the barrier) $G_0 = (\pi/2)\tau_0^2 L/\mu$.
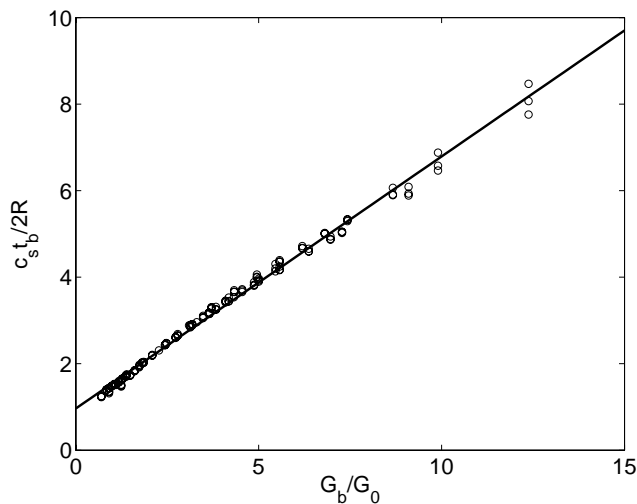

Figure 3. Scaling for barrier break time for a spontaneous, dynamic model with periodic boundary conditions in the vertical direction (no free surface) and constant prestress everywhere on the fault.
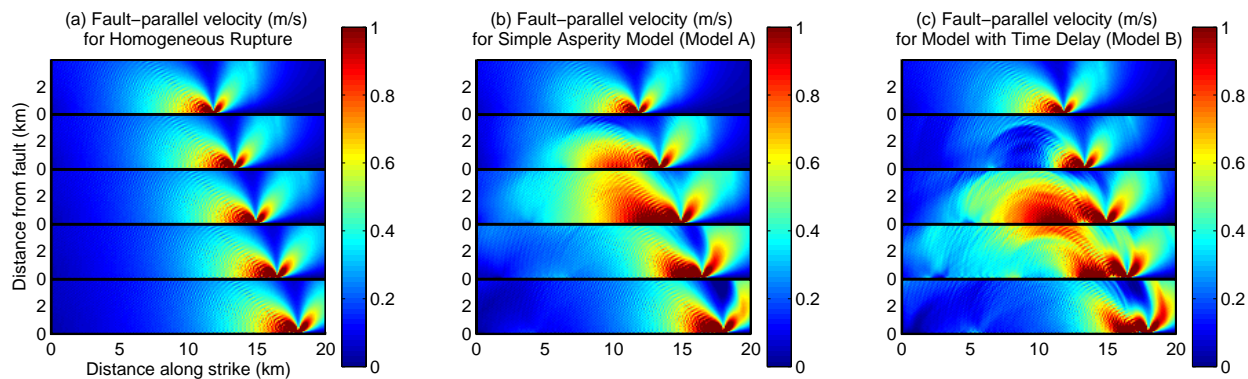

Figure 4. Fault-parallel velocity on the surface at 0.56 second intervals for several models with constant rupture velocity. The homogeneous rupture (a) has no stress heterogeneity and is shown as a reference. The additional burst of radiation due to the heterogeneity can be seen in Model A (b). The barrier time delay of 0.28 seconds in Model B (c) initially arrests the ground motion, producing arrest waves visible in the second panel, followed by a more dramatic pulse when the barrier fails. These features are most easily seen in the fault-parallel components. In the fault-perpendicular records, the homogeneous pulses dominate the motion, as seen in Figure 2. In these plots $\tau_b = 35$ MPa, $R = 1$ km, and $d = 5$ km. Note that the color scale is clipped for points close to the fault.

The break time is scaled by the time it takes a shear wave to cross the barrier $2R/c_s$. In these expressions, c_s is the shear wave speed, d_c is the slip-weakening displacement, τ_0 is the prestress (which is constant everywhere), and τ_y^b is the yield stress of the barrier.

Figure 3 shows the results of 150 numerical experiments, revealing that the break time scales linearly with G_b/G_0. This result arises from a balance between the energy driving the rupture (proportional to G_0) and that resisting it (proportional to G_b). This balance of energies has been discussed by *Madariaga and Olsen* [2000] and G_b/G_0 is, up to a constant, equal to the inverse of their parameter κ, which has been shown to determine the rupture dynamics of homogeneous faults. A linear fit between the nondimensionalized break time and resistance of the barrier yields

$$t_b = \frac{2R}{c_s}(1 + 0.6\frac{G_b}{G_0}). \qquad (3)$$

In Section 3, we extend this analysis to the case of a finite fault bounded on top by a free surface.

Returning to Model B, we specify that the heterogeneity, now more like a barrier, again fails with a straight rupture front, but at a later time. This delay time makes the ground motion more dramatic: As the rupture front passes around the unbroken barrier, the stress within it increases, particularly at the edges of the unbroken region. As the barrier rupture delay approaches infinity, the stress buildup in the barrier approaches the initial conditions of the Das-Kostrov asperity model, in which the rest of the fault is broken [*Das and Kostrov*, 1983]. Due to the additional stored stress, the barrier in this model breaks more violently than in the first model without the time delay.

Figure 4 shows the changes in ground motion introduced by a time delay of 0.28 seconds. Unlike in Model A, the barrier in Model B, which is initially locked as the rupture front surrounds it, first arrests the ground motion producing a stopping phase visible in the second panel. When the barrier does fail, it produces a pulse that reaches the surface at a later time than in Model A. The peak velocity in this pulse is higher than in Model A as well. Thus the time delay leads to larger velocities in the seismograms, not because the initial conditions of the models are different (they are not – the prestress is the same in Model A and Model B) but due to the additional stress stored in the barrier region as the rupture front surrounds it.

In Model C, the final reduced model, we attempt to more closely match the spontaneous breaking of the barrier. Due to the increased stress around the edge of the barrier, in the spontaneous case the barrier collapses inward with a curved rupture front [*Das and Kostrov*, 1983]. The curved rupture front focuses the energy to a point, so that the barrier breaks with a well-defined pulse. To mimic this, we specify the rupture front as an arc with the same radius of curvature as the barrier itself, moving in the forward direction across the barrier with a fixed rupture velocity v_r. This model also has a barrier time delay. In comparison to Model D, we find that the motion on the fault is similar, although in the spontaneous dynamic case the radius of curvature of the rupture front decreases as the barrier breaks. Thus in the spontaneous dynamic case there is even more focusing, leading to a very well-defined pulse as the last area of the barrier fails. The spontaneous dynamic results are discussed more completely in Section 3.

3. Spontaneous Dynamic Model

Finally, we consider Model D, a fully spontaneous, dynamic model governed by a linear slip-weakening friction law [*Ida*, 1972; *Palmer and Rice*, 1973; *Andrews*, 1976]. We

specify a slip-weakening displacement of $d_c = 0.47$m. A circular heterogeneity with radius 1 km is located 10 km along strike and at a depth of 5 km. In this model, the rupture velocity is allowed to vary. The dynamic model also allows a different degree of freedom, for both the yield stress and prestress are specified at each point. Outside the heterogeneity, we choose a background prestress of 5 MPa and a yield stress of 10 MPa. Rupture is initiated by raising the prestress along a vertical patch at one side of the fault.

The dynamic parameters in the heterogeneity can be tuned to make an asperity-like model (high prestress) or a barrier-like model (high yield stress). For the "representative" asperity rupture in the following figures we choose an asperity prestress of 35 MPa and an asperity yield stress of 40 MPa. The examples plotted of a barrier rupture use a barrier prestress of 5 MPa and yield stress of 50 MPa.

For asperity-like models, the ground motion is very similar initially to the reduced models without a time delay. However, a sufficiently large prestress can initiate supershear rupture, forming a second pulse on the free surface. Barrier-like models have a similar rupture history to the reduced models with time delay. However, we find that in both cases, the dynamic models produce more ground motion than the reduced models with similar rupture history and equivalent stress drop. The change in ground motion introduced by constraining rupture velocity can be seen in Figure 5. The black seismograms in this figure show the fault-parallel velocity from a fully dynamic, spontaneous rupture (Model D).
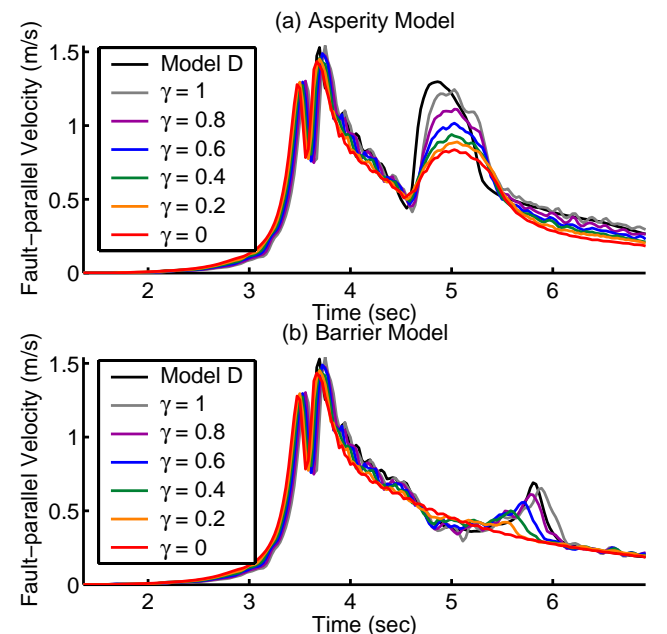

Figure 5. The effect of a rupture-velocity constraint at a station 0.5 km off-fault from the surface point directly above the heterogeneity. The nondimensional parameter γ is a measure of the amount of variation in rupture velocity that is allowed. (A complete description is given in the text.) The black lines are velocity seismograms for a spontaneous, dynamic rupture (Model D) with no rupture-velocity constraint for a rupture with an asperity (a) and a barrier (b). The rupture history of these runs can be approximated by a constrained model shown in gray. As we constrain the rupture velocity to be more constant (and decrease γ), the barrier and asperity pulses shrink, until we reach the red line, which shows a fully constrained model where rupture velocity is constant everywhere and the rupture front is straight (Model A).

To understand the remaining seismograms in Figure 5, first consider a point on the fault a horizontal distance x from the nucleation zone in Model D that has a rupture time of t'. In a fully constrained model with constant rupture velocity (Model A), this point has a rupture time of x/v_r. Therefore $x/v_r - t$ is the time perturbation necessary to force the point in the constrained model to rupture at the same time as it does in the spontaneous rupture. We can approximate the spontaneous rupture with a constrained model by considering t in Equation 2 a function of position. If we make the substitution $t \rightarrow t + \gamma(x/v_r - t')$ for each point on the fault, when $\gamma = 1$ we have a constrained rupture that approximates the rupture history of the fully dynamic, spontaneous rupture. As we decrease γ, the rupture velocity is more and more constrained, until $\gamma = 0$, giving a constant rupture-velocity and a straight rupture front (Model A, shown in red). Note that the red seismograms for the asperity and barrier ruptures are different due to the difference in pre-stress within the heterogeneities between the two models. Figure 5 shows that in both the asperity and barrier cases, the more constrained the rupture velocity, the smaller the pulses from the heterogeneity, even though for a given case (asperity rupture or barrier rupture), the prestress is the same in both the constrained and in the spontaneous models. This is true even though the perturbation to the rupture time $x/v_r - t'$ is positive in the asperity region and negative in the barrier region. The result is the same – constraints in rupture velocity (in this case, limits on both rupture-front curvature and variations in rupture velocity) lead to less ground motion. This suggests that a kinematic model that introduces such a constraint would give an upper limit on τ_b. Smoothing about a particular rupture velocity in an inversion, in effect, sets a scale for stress. This leads to an overestimation of stress heterogeneity on the fault.

Figure 6 shows fault-parallel particle velocity (half of the slip rate) on the fault plane as well as fault-parallel velocities on the free surface for two Model D ruptures. The first panel is shown 3.75 seconds after nucleation, and subsequent panels are plotted at 0.69 second intervals. The rupture with an asperity has a very different rupture history than the rupture with a barrier, and this causes differences in the ground motion as well. The asperity rupture produces a large super-shear pulse traveling ahead of the (original) rupture front. This happens in the barrier case as well, but the supershear pulse is much smaller and dies out quickly. In the asperity rupture, the supershear rupture leads to a Mach front that is visible on the surface further down the fault. The breaking of the barrier produces a very well-defined interface wave
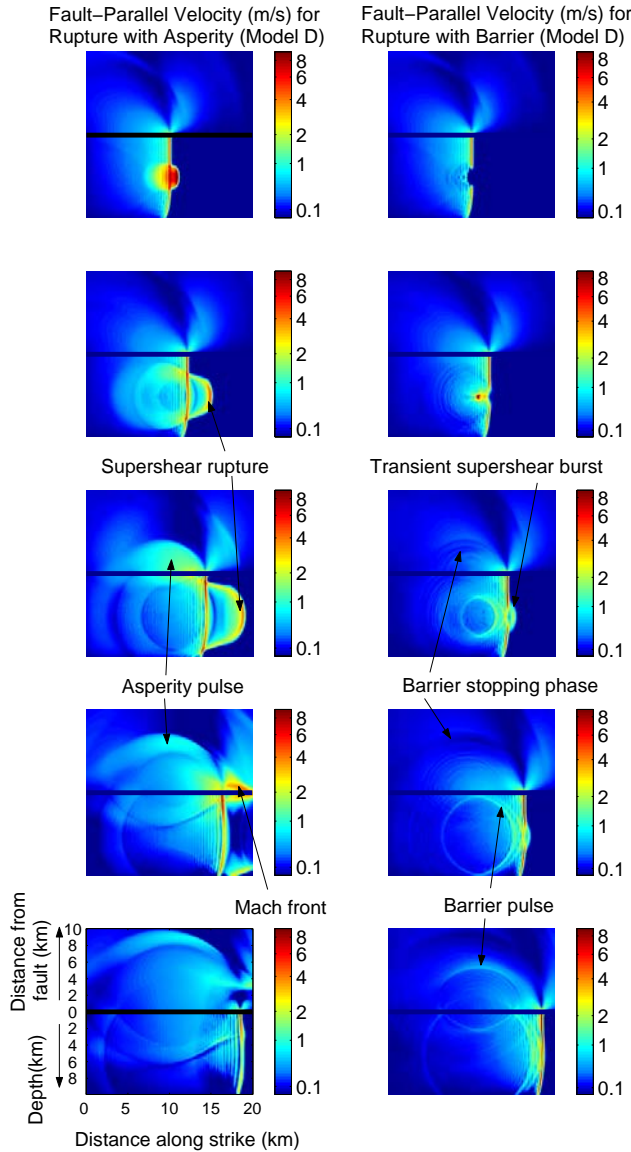

Figure 6. Comparison of fault-parallel velocity for two spontaneous, dynamic models (Model D). The horizontal black line in each diagram represents the fault trace on the surface. Above this line, fault-parallel velocity is plotted on the free surface. Below this line, fault-parallel particle velocity on the fault plane is shown. (These planes are perpendicular to each other as shown in Figure 1.) Note that the color scale is logarithmic.
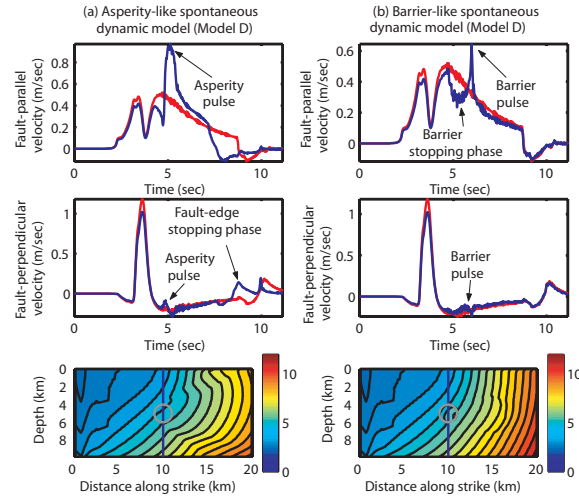

Figure 7. Seismograms and isochrones for two spontaneous, dynamic models. The blue seismograms show the radiation produced for a point 2 km off-fault from the point directly above the center of the heterogeneity. The red seismograms are from a homogeneous rupture with the same background prestress and yield stress as the heterogeneous ruptures and are shown as a reference. The lower plots show S-wave isochrones for the heterogeneous ruptures at this particular station. The contours are plotted at 0.5 second intervals. The vertical blue line shows the projection of the station location onto the fault, and the gray circle shows the location of the heterogeneity.

that travels unhindered along the previously broken regions of the fault. In the asperity rupture, there is less rupture-front focusing, and thus the asperity pulse is less well-defined than the barrier pulse. The main differences in the ground motion can be seen in the wave arrival times and the stopping phase from the initial delay in rupture of the barrier region. In particular, a large asperity can produce extremely high fault-parallel velocities. The signature of a barrier is most clearly seen in the rupture history on the fault, and thus, in wave arrival times on the surface.

Sample seismograms and their corresponding S-wave isochrones for Model D are shown in Figures 7 and 8. The isochrones show which parts of the fault are contributing to the ground motion seen at various times for a given station [*Bernard and Madariaga*, 1984; *Spudich and Frazer*, 1984]. Radiation is quite different for the asperity and barrier rup-

tures. In the barrier rupture, the barrier initially resists rupture, and this can be seen in the isochrones and in stopping phases visible in the seismograms. The highly loaded asperity, however, generates supershear rupture velocities, which dramatically alter the isochrones in the forward direction from the asperity. Also, the asperity pulse width is much greater than the barrier pulse width due to rupture-front focusing in the barrier rupture.

One can invert for the prestress and yield stress of the heterogeneity, relative to friction, from only two parameters: the break time of the heterogeneity and the final fault-parallel offset on the surface. The break time, which can be found from a kinematic inversion or simple timing of wave arrivals, increases with fracture energy. The fault-parallel static offset at all points on the surface is a monotonically increasing function of dynamic stress drop. Contours for each of these parameters for different levels of prestress and yield stress in the barrier are shown in Figure 9. This plot shows the results of 45 numerical experiments, each with a different prestress and yield stress for the barrier. Note that the static-offset contours are drawn for a particular point on the surface, 0.5 km off-fault from the point directly above the barrier center. However, the contours were found to be similar for all near-field points. Any one station is sufficient for this constraint, for all stations have offsets that are increasing functions of prestress alone.

Note that in Figure 9, displacement is no longer a linear function of prestress (that is, the contours for prestress are not spaced evenly), as in the reduced models. Also, barrier time delay is no longer proportional to fracture energy, as found in the simpler case with periodic boundary conditions and constant prestress (Figure 3). However, since final displacement is independent of yield stress (as the vertical contours in Figure 9b show), these two parameters can be used together to determine both dynamic parameters. Furthermore, the monotonicity of each parameter gives the direction to search, and guarantees that the solution found will be unique. Given enough stations to resolve barrier break time, the dynamic parameters of a simple barrier are fully constrained. In these models, we have left the slip-weakening displacement, d_c, constant. Due to the trade-off between d_c and strength excess [*Guatteri and Spudich*, 2000], we cannot constrain d_c as well.

As the barrier size decreases, the dynamic scaling relations become linear. When the radius of the barrier is small compared to the fault depth, fault-parallel static offset is linear in prestress and the time delay is a linear function of strength excess. Also, in the small barrier limit, the final offset again scales with R^2, as was the case in the original model with fixed rupture velocity. For a smaller barrier, however, the change in static offset may not be resolvable. A barrier with $R = 1$ km and a prestress of 40 MPa increases the fault-parallel static offset by 17% for a point close to the fault (Figure 9b). If the radius is instead 0.35 km, the static offset change becomes negligible at 2%. This is the main limitation of our result: a strong heterogeneity is required to provide the resolution to determine both the prestress and yield stress of the barrier.
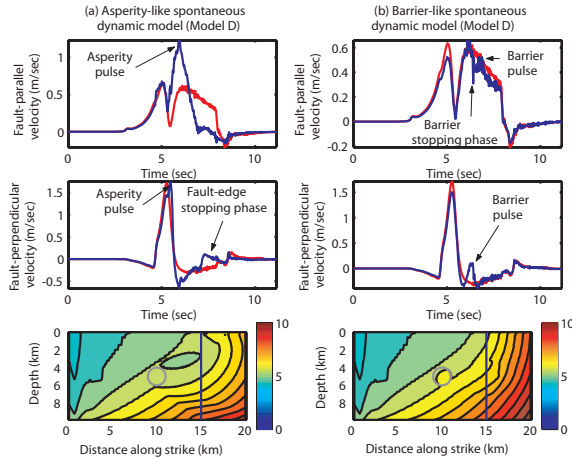

Figure 8. Seismograms and isochrones for two spontaneous, dynamic models in the format of Figure 7. Here the seismograms and isochrones are shown for a point 2 km from the fault and 5 km in the forward direction from the heterogeneity. The vertical blue line in the bottom panels shows the projection of the station location onto the fault.
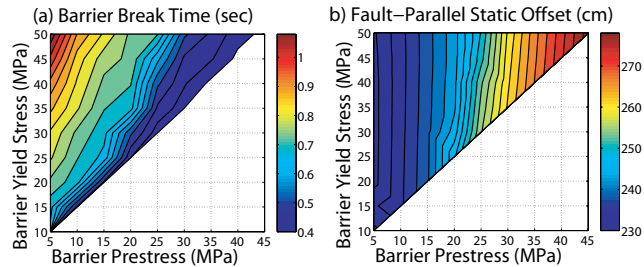

Figure 9. Contours of barrier break time (a) and final fault-parallel offset (b) for spontaneous, dynamic models (Model D). The contours for static offset are plotted 0.5 km off-fault from the point directly above the barrier center. The lowest data point in these plots represents a homogeneous rupture, where the barrier region has the same prestress and yield stress as the background. The vertical contours for the static offset show that offset is a function of prestress alone. Also, since the contours for the break time have a different slope, break time and static offset can be used together to constrain prestress and yield stress.

4. Conclusion

With a series of increasingly complex models, we have analyzed the radiation produced by barriers and asperities. We found that a delayed barrier break time initially arrests the rupture, leading to stronger ground motion when the barrier eventually fails. In addition, rupture-front focusing leads to a sharper barrier pulse on the surface, which is even more pronounced in spontaneous models. We found that the pulses generated by heterogeneities were most clearly seen

in the fault-parallel component. Here, the heights of the velocity pulses help to constrain the size and strength of the heterogeneity, while the width of the pulses constrain size and depth. If the fault-perpendicular asperity or barrier pulses can be resolved, their polarity gives the location of the heterogeneity.

We also investigated the scaling in a fully spontaneous, dynamic model. The static offset and barrier break time allow both dynamic parameters, prestress and strength, to be constrained for the case of a circular barrier on an otherwise homogeneous fault. This is primarily because prestress controls static offset, while strength excess controls the break time of the barrier.

In this paper, we have studied simplified rupture scenarios in order to derive general results. Real earthquakes are likely to be considerably more heterogeneous than our models. However, these results could be used to help guide kinematic inversions for earthquakes that are relatively homogeneous with the exception of a large stress drop in a concentrated region. One possible candidate is the 1984 Morgan Hill earthquake. A kinematic inversion by Beroza and Spudich *Beroza and Spudich* [1988] found a barrier region 13 km southeast of the hypocenter. This region initially resisted rupture, and produced high slip when it failed. This barrier, however, may have failed in the opposite direction as the rest of the earthquake, as a large late pulse at a station in the backward direction suggests that the directivity from this region was to the back [*Beroza and Spudich*, 1988]. This is somewhat more complicated than the type of rupture considered in this paper.

Also, we found that constraints on rupture velocity significantly affect ground motion. Restrictions that lead to less rupture-velocity variation and less rupture-front curvature dampen the pulses seen in ground-motion. This suggests that kinematic inversions with rupture velocity constraints will overestimate the actual stress heterogeneity. The unconventional approach in this paper – starting with a highly simplified, constrained model, and adding back in the elements of a fully dynamic, spontaneous rupture, as opposed to the conventional, kinematic approach of approximating a fully dynamic rupture with a complex, but fully-constrained rupture – allows the effects of these constraints and simplifications to be clearly seen. This is important because kinematic inversions are by far the most computationally practical way to invert for the earthquake source. At the same time, they are underdetermined, and can be unphysical. We must be aware of the effects of constraints that are (of course, must be) imposed in kinematic inversions. Ideally, these constraints will lead to ruptures that are physical and consistent with dynamic ruptures as well.

References

Andrews, D. J. (1976), Rupture velocity of plane strain shear cracks, *J. Geophys. Res.*, *81*(32), 5679–5687.

Andrews, D. J. (1985), Dynamic plane-strain shear rupture with a slip-weakening friction law calculated by a boundary integral method, *Bull. Seismol. Soc. Am.*, *75*(1), 1–21.

Archuleta, R. J. (1984), A faulting model for the 1979 Imperial Valley earthquake, *J. Geophys. Res.*, *89*(B6), 4559–4585.

Bernard, P., and R. Madariaga (1984), A new asymptotic method for the modeling of near-field accelerograms, *Bull. Seismol. Soc. Am.*, *74*(2), 539–557.

Beroza, G. C., and P. Spudich (1988), Linearized inversion for fault rupture behavior: Application to the 1984 Morgan Hill, California, earthquake, *J. Geophys. Res.*, *93*(B6), 6275–6296, doi:10.1029/88JB01405.

Cotton, F., and M. Campillo (1995), Frequency domain inversion of strong motion: Application to the 1992 Landers earthquake, *J. Geophys. Res.*, *100*(B3), 3961–3975, doi: 10.1029/94JB02121.

Das, S., and K. Aki (1977), Fault plane with barriers: A versatile earthquake model, *J. Geophys. Res.*, *82*, 5658–5670.

Das, S., and B. V. Kostrov (1983), Breaking of a single asperity: Rupture process and seismic radiation, *J. Geophys. Res.*, *88*, 4277–4288.

Dunham, E. M., P. Favreau, and J. M. Carlson (2003), A supershear transition mechanism for cracks, *Science*, *299*(5612), 1557–1559, doi:10.1126/science.1080650.

Fukuyama, E., and R. Madariaga (2000), Dynamic propagation and interaction of a rupture front on a planar fault, *Pure Appl. Geophys.*, *157*, 1959–1979.

Geller, R. J. (1976), Scaling relations for earthquakes source parameters and magnitudes, *Bull. Seismol. Soc. Am.*, *66*, 1501–1523.

Guatteri, M., and P. Spudich (2000), What can strong-motion data tell us about slip-weakening fault-friction laws?, *Bull. Seismol. Soc. Am.*, *90*(1), 98–116, doi:10.1785/0119990053.

Hartzell, S. H., and T. H. Heaton (1983), Inversion of strong ground motion and teleseismic waveform data for the fault rupture history of the 1979 Imperial Valley, California, earthquake, *Bull. Seismol. Soc. Am.*, *73*(6), 1553–1583.

Ida, Y. (1972), Cohesive force across the tip of a longitudinal-shear crack and Griffith's specific surface energy, *J. Geophys. Res.*, *77*, 3796–3805.

Kostrov, B. V., and S. Das (1988), *Principles of earthquake source mechanics*, 132-138,166 pp., Cambridge University Press, Cambridge.

Madariaga, R. (1978), The dynamic field of Haskell's rectangular dislocation fault model, *Bull. Seismol. Soc. Am.*, *68*(4), 869–887.

Madariaga, R. (1983), High frequency radiation from dynamic earthquake fault models, *Ann. Geophys.*, *1*(1), 17–23.

Madariaga, R., and K. B. Olsen (2000), Criticality of rupture dynamics in 3-d, *Pure Appl. Geophys.*, *157*, 1981–2001.

Olson, A. H., and R. J. Apsel (1982), Finite faults and inverse theory with applications to the 1979 Imperial Valley earthquake, *Bull. Seismol. Soc. Am.*, *72*(6), 1969–2001.

Palmer, A., and J. R. Rice (1973), The growth of slip surfaces in the progressive failure of over-consolidated clay, *Proc. R. Soc. London Ser. A*, *332*(1591), 527–548.

Peyrat, S., K. B. Olsen, and R. Madariaga (2001), Dynamic modeling of the 1992 Landers earthquake, *J. Geophys. Res.*, *106*(B11), 26,467–26,482, doi:10.1029/2001JB000205.

Peyrat, S., K. B. Olsen, and R. Nirmal (2004), Nonlinear dynamic inversion of the 2000 Western Tottori, Japan, earthquake, *Geophys. Res. Lett.*, *31*, L05604, doi:10.1029/2003GL019058.

Somerville, P., et al. (1999), Characterizing crustal earthquake slip models for the prediction of strong ground motion, *Seism. Res. Lett.*, *70*(1), 59–80.

Spudich, P., and L. N. Frazer (1984), Use of ray theory to calculate high-frequency radiation from earthquake sources having spatially variable rupture velocity and stress drop, *Bull. Seismol. Soc. Am.*, *74*(6), 2061–2082.

Wald, D. J., and T. H. Heaton (1994), Spatial and temporal distribution of slip for the 1992 Landers, California earthquake, *Bull. Seismol. Soc. Am.*, *84*(3), 668–691.

Morgan T. Page, Department of Physics, University of California at Santa Barbara, Santa Barbara, CA 93106-9530, USA. (pagem@physics.ucsb.edu)

Eric M. Dunham, Department of Earth and Planetary Sciences, Harvard University, Cambridge, MA 02138, USA. (edunham@fas.harvard.edu)

J. M. Carlson, Department of Physics, University of California at Santa Barbara, Santa Barbara, CA 93106-9530, USA. (carlson@physics.ucsb.edu)